9 (2): 277-284 (2025)

Journal of Aviation

https://dergipark.org.tr/en/pub/jav

e-ISSN 2587-1676

Computational Evaluation of Aerodynamics and Aeroacoustics of a Propeller for a Multirotor Unmanned Aerial Vehicle

Yahya Çelebi[1*], Ahmet Aydın[2], Selman Aydın[3]

[1*]Şırnak University, Department of Motor Vehicles and Transportation Technologies, Şırnak, Türkiye, 73000. (yahya.celebi@outlook.com)
[2] Nişantaşı University, Department of Mechatronics Engineering, İstanbul, Türkiye, 34398. (aydin.ahmet@nisantasi.edu.tr)
[3] Batman University, Department of Mechanical and Metal Technology, Batman, Türkiye, 72060. (selman.aydin @batman.edu.tr)

Article Info

Received: 13 February 2025
Revised: 22 May 2025
Accepted: 11 June 2025
Published Online: 22 June 2025

Keywords:
Aerodynamic
APC 9x4.5
UAV
Propeller
Aeroacoustic
CFD

Corresponding Author: *Yahya Çelebi*

RESEARCH ARTICLE

https://doi.org/10.30518/jav.1638955

Abstract

The development of aircraft propulsion systems requires a comprehensive understanding of propeller performance characteristics under various operating conditions. While experimental testing traditionally provides reliable data for propeller performance curves at different cruising speeds and rotational velocities the associated costs and time investments have driven researchers toward alternative evaluation methods including computational and analytical approaches. This research presents a detailed computational investigation of a quadrotor unmanned aerial vehicles propeller focusing on two critical performance aspects thrust coefficient variation and aeroacoustic behaviour. The study employed computational fluid dynamics simulations to analyze a 9-inch propeller under vertical climbing conditions examining multiple advance ratios and rotational speeds. Computational accuracy was ensured through mesh independence studies which determined the optimal discretization of the solution domain. The CFD results demonstrated strong correlation with experimental data regarding thrust coefficient predictions, thereby validating the computational approach. The aeroacoustic analysis revealed favourable noise characteristics with the propeller maintaining consistently moderate sound pressure levels across all measured angular positions. These findings validate both the effectiveness of the computational methodology and confirm the balanced performance of the propeller design in terms of both aerodynamic efficiency and noise generation.

1. Introduction

The revolution in autonomous flight technology continues to expand as Unmanned Aerial Vehicles (UAVs) transform industries by providing cost-effective solutions and versatile deployment options (Çelebi and Aydın, 2025a). These vehicles are widely used in research applications where they enable rapid data collection and reduce research team workload (Ciattaglia et al., 2023). In addition, the economic benefits are significant, as UAV operations can cost merely 20% of what conventional aircraft operations cost (Cruzatty et al., 2022). Moreover, recent advances in communications, sensor technology, and computing power have enabled further widespread adoption and increasingly sophisticated applications of UAVs (Al-Haddad et al., 2024; Yıldırım Dalkıran and Kırteke, 2024). The convergence of electronic miniaturization and aerospace engineering innovations has driven the aerial vehicle industry to unprecedented growth, with market valuations reaching $25.6 billion in 2021 and forecasts indicating continued expansion (J. Lu et al., 2025). UAVs are available in various configurations and sizes. While small-sized UAVs consist of handheld devices equipped with cameras and sensors, larger variants typically feature fixed wings that allow for extended travel distances (Özen and Oktay, 2024). These aircraft can be configured with different propeller arrangements, including quadcopters, hexacopters, octocopters and so on. Despite the variety in configurations, these systems typically rely on multiple conventional propellers rotating in the parallel planes to generate thrust (McKay et al., 2021).

A critical consideration in UAV design and construction is achieving optimal performance, which encompasses flight time, load capacity, maximum travel distance, and speed capabilities (Nikolaou et al., 2025). For multirotor configurations, propellers serve as the primary source of lift, making their performance characteristics, including thrust and power crucial for achieving efficient design outcomes (Jordan et al., 2020). However, small-scale propellers encounter viscous effects that significantly reduce their performance metrics, including payload capacity, range, and endurance, when operating under low Reynolds number conditions (Oktay and Eraslan, 2020). While propeller drive systems remain the most effective propulsion solution for both electric and fuel-powered air vehicles. High-altitude air vehicles with propeller systems can operate from ground level to an attitude of 25,000 meters. However, propeller design for such high-altitude aircraft propulsion systems presents significant engineering challenges due to dramatically varying operating conditions. These conditions include substantial changes in air density which can vary by a factor of ten, resulting in low Reynolds numbers below 1.0×10^5 and relatively slow advance velocities between 10 to 30 m/s (You et al., 2020). Beyond performance considerations, propeller noise has historically been a significant community concern, particularly in areas

with high air traffic such as airports and urban areas (Del Duchetto et al., 2025). The recent surge in popularity of drones and other UAVs for urban applications, such as package deliveries and surveillance, has further intensified research into propeller noise mitigation and the development of quieter devices and advanced noise reduction systems (de Carvalho et al., 2023).

Airfoils represent specialized wing profiles utilized in various applications including fixed-wing aircraft, helicopter rotor blades, wind turbines, fans, and propeller blades. Well-designed airfoil configurations typically deliver optimal performance characteristics in terms of lift, drag, aerodynamic efficiency, and stability (Durmuş, 2024). Advanced computational simulations enable comprehensive aerodynamic shape optimization to identify designs that maximize aerodynamic performance. The term low-Reynolds-number refers to flow conditions where the chord Reynolds number is below 1.0×10^6. Most UAVs operate within this flow regime, specifically in the range of 1.0×10^5 to 1.0×10^6 (Li et al., 2022).

In the literature, numerous studies have employed CFD methodologies to examine multicopter UAV propeller aerodynamic characteristics. Oktay and Eraslan (Eraslan and Oktay, 2021) conducted comprehensive computational studies exploring how rotational speed parameters affect thrust and aerodynamic performance. Their work with an 11-inch 4.7 pitch-ratio propeller demonstrated that increasing rotational speed enhanced turbulent kinetic energy during vertical climb. The research revealed that while faster rotation speeds caused larger discrepancies between computational and experimental data, it simultaneously reduced airspeed sensitivity. You et al. (You et al., 2020) investigated an optimized propeller design for a solar UAV operating at 22 km altitude, aiming to maximize aerodynamic performance through advanced CFD analyses. Design specifications for the three-blade propeller included a target efficiency of 72% and thrust of 7 N, operating with a diameter of 0.5588 m at 5500 rpm in 50 m/s freestream conditions. They selected the FX 63-137 airfoil for its optimal lift-to-drag ratio at the specified altitude. The final design achieved 70.49% efficiency and successfully met the thrust requirements. Ahmad et al. (Ahmad, Kumar, Pravin, et al., 2021) compared three distinct propeller designs using Ansys software for modal analyses. Using carbon fiber reinforced polymer as the material, they evaluated and compared the designs based on natural resonance frequencies and maximum deformation characteristics. In a separate study, Ahmad et al. (Ahmad, Kumar, Dobriyal, et al., 2021) analyzed flow characteristics around a quadcopter propeller to determine thrust coefficient using Ansys software with the k-epsilon turbulence model at various angular speeds. Their results confirmed that the propeller could generate sufficient thrust for additional payloads. Cespedes and Lopez (Céspedes and Lopez, 2019) simulated a single rotor using the overset mesh technique in Ansys Fluent v19, assuming incompressible and turbulent flow conditions. The computational results correlated well with experimental measurements, with thrust prediction discrepancies remaining below 7% and torque requirements varying by approximately 22%. Upon scaling to four rotors, they observed a 5% decrease in thrust per rotor and a 3% increase in required torque.

The performance evaluation of a propeller typically requires comprehensive analysis of the thrust coefficient (C_T) and advance ratio (J). These fundamental parameters are defined through Equations (1 and 2) (Anh Vu et al., 2025). In these expressions, T represents thrust in Newtons, ρ denotes air density in kg/m^3, n denotes revolutions per second in rps, V represents the air velocity in m/s, and D indicates propeller diameter in meters. The relative percentage error calculations for C_T can be determined using Equations 3 (Çelebi and Aydın, 2025b).

$$C_T = \frac{T}{\rho n^2 D^4} \quad (1)$$

$$J = \frac{V}{nD} \quad (2)$$

$$\Delta C_T(\%) = \frac{C_{T,Exp.} - C_{T,CFD}}{C_{T,Exp.}} x100 \quad (3)$$

Three primary approaches exist for CFD simulations of turbulent flows: Direct Numerical Simulation (DNS), Large Eddy Simulation (LES), and Reynolds-averaged Navier–Stokes (RANS) (Jin et al., 2025). DNS resolves all turbulent scales down to the smallest dissipating eddies, but its computational demands make it impractical for most engineering applications. RANS equations, while computationally efficient, are inadequate for aeroacoustic simulations because they time-average the turbulent fluctuations that serve as critical sources of aerodynamic noise. LES provides a middle-ground approach that directly computes the large-scale, anisotropic turbulent motions responsible for energy transport while modeling the smaller, more isotropic subgrid-scale structures through appropriate closure models (Lasota et al., 2021). This methodology captures the unsteady turbulent characteristics essential for accurate aeroacoustic predictions while maintaining reasonable computational costs.

The existing literature reveals a substantial research gap in comprehensive performance analysis of small-scale UAV propellers, particularly regarding the integration of aerodynamic and aeroacoustic characteristics. While numerous studies have examined individual aspects of propeller performance, relatively few have provided integrated analysis across multiple operating conditions. This study aims to address this gap by conducting a detailed CFD investigation of the APC 9x4.5 propeller, focusing on both aerodynamic performance and noise generation characteristics. The research objectives encompass systematic evaluation of thrust coefficient variations across diverse advance ratios and rotational speeds, validation of computational predictions against experimental data, and acoustic performance through sound pressure measurements at various angular positions. This approach provides essential insights for UAV designers and manufacturers, particularly in applications where both performance optimization and noise reduction are equally critical.

2. Numerical methods

In this study, ANSYS Fluent software was utilized. This software performs CFD analysis through three main steps through pre-processing, solving and post-processing. During the pre-processing phase, the computer aided design (CAD) model of the propeller was imported into Ansys SpaceClaim. For this study, the Advanced Precision Composites (APC) Thin Electric 9x4.5 propeller (a 9-inch diameter and 4.5-inch pitch) was used. This specific model has been extensively

employed in UAV applications, and its geometrical data and experimental performance data were published by Brandt (Brandt, 2005). **Figure 1** presents APC Thin Electric 9x4.5 geometrical characteristics.

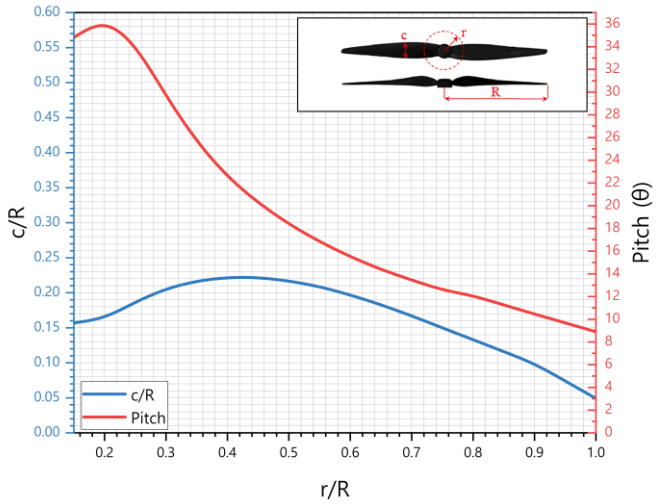

Figure 1. APC Thin Electric 9x4.5 geometrical characteristics.

The CAD model was created in Solidworks and imported into the Ansys design tool to create and define computational domains around the propeller. Figure 2 provides a detailed view of the APC Thin Electric 9x4.5 test propeller.

Figure 2. APC Thin Electric 9 inches 4.5 inches propeller blade.

The flow analysis employs a Multiple Reference Frame model to characterize propeller aerodynamics. Ansys SpaceClaim facilitated domain construction with dual reference frames centered around the propeller. The computational space consists of three distinct cylindrical regions with specific dimensional relationships to the propeller diameter. The outer domain serves as the stationary reference frame, extending up to 20 times the propeller diameter in the axial direction and 10 times in the radial direction. This strategically generous boundary placement ensures undisturbed flow development. The rotating domain, functioning as the moving reference frame, was dimensioned at 1.1 times propeller diameter radially and 0.1 times diameter axially. The inner domain was designated as the Body of Interest (BOI) and located downstream of the propeller. Its domain size was equivalent to propeller diameter in order to obtain a refined mesh for analyzing airflow. Figure 3 presents the complete flow domain configuration showing both reference frames.

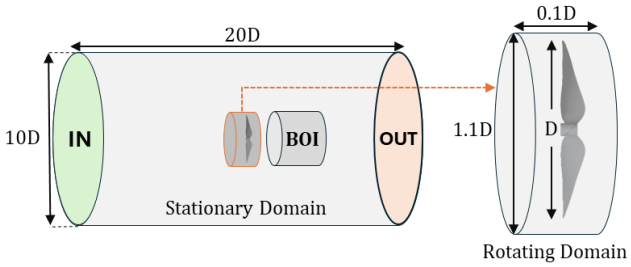

Figure 3. Flow domain and boundary conditions.

The computational mesh was generated in ANSYS Fluent Meshing using poly-hexcore elements. This advanced meshing strategy significantly reduces total element count while simultaneously accelerating solution convergence (Çelebi and Aydın, 2025b). The mesh structure features refined density near propeller surfaces to capture critical flow phenomena. Element size transitions gradually from high resolution at the propeller surface to coarser spacing in the outer domain regions. Figure 4 displays the detailed surface mesh distribution across the propeller geometry.

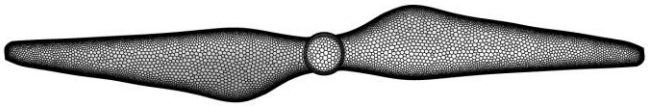

Figure 4. View of the mesh distribution on the propeller surface.

The initial boundary layer mesh spacing follows a specific mathematical relationship defined in Equation 4. This equation determines the first layer thickness (y) based on the dimensionless wall distance (y+) and fluid dynamic viscosity (μ) (Çelebi et al., 2024). This precise calculation ensures adequate resolution of near-wall flow phenomena. The mesh distribution near the propeller is shown in Figure 5.

$$y = \frac{y^{+}\mu}{\rho u_{*}} \tag{4}$$

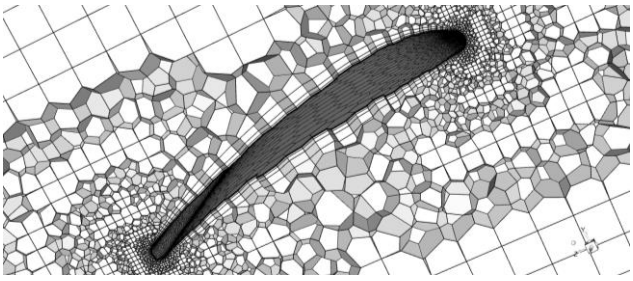

Figure 5. Mesh near the propeller.

CFD accuracy verification relies on mesh independence analysis to ensure solution stability. This process validates result consistency across varying mesh densities while optimizing computational efficiency. The methodology begins with a standard low-element model, progressively increasing mesh density until results demonstrate convergence. The independence study focused on specific operating conditions: 4002 rpm rotational speed and 2.9732 m/s velocity. The computational model incorporated as the propeller and hub surfaces using no-slip wall conditions. The k-ω SST turbulence model was chosen, incorporating curvature correction. This advanced model includes adjustments for low-

Reynolds number effects, compressibility, and the spreading of shear flows. The air density and viscosity were set to correspond to standard sea-level atmospheric conditions. Table 1 provides a comprehensive listing of all boundary condition parameters applied to the simulation domains.

Table 1. Boundary conditions for validation.

Property	Value
Turbulence model	SST k-omega
Fluid	Air
The density of fluid (kg/m^3)	1.225
Inlet velocity (m/s)	2.9732
Rotational speed (rpm)	4002
Outlet pressure (Pa)	0
Propeller domain	'None Slip Wall' condition

Mesh independence studies were conducted to ensure computational accuracy while optimizing efficiency. The mesh density was varied by adjusting the number of elements along both the blade span and chord directions, resulting in computational mesh ranging from 8 to 13 million nodes. Multiple mesh configurations with different element sizes were tested to determine the optimal mesh resolution. Table 2 presents the detailed mesh quality metrics and element sizes from the independence analysis.

Table 2. Mesh quality and numerical data for mesh independence for 4002 rpm and 0.195 J.

Mesh	Cells	Faces	Nodes	Skewness	Orthogonal quality
Fine	4,215,931	20,506,627	13,182,036	0.849	0.150
Coarse	3,781,820	18,302,413	11,704,791	0.847	0.150
Standard	2,123,444	11,576,597	8,202,012	0.850	0.150

Performance evaluation at a 0.195 advance ratio and 4002 rpm was conducted to establish mesh sensitivity characteristics. The mesh independence study revealed minor variations in thrust measurements across different mesh densities. The variation in key flow parameters between the coarse and fine meshes was less than 1%, indicating that mesh resolution had minimal impact on solution accuracy within this range. Based on these findings, the mesh with the lowest node count was selected for the final simulations, as it provided adequate accuracy while minimizing computational cost. Table 3 presents the complete set of performance variations observed during mesh refinement testing.

Table 3. CFD results at different mesh resolutions for 4002 rpm and 0.195 J.

Mesh	Thrust (N)	C_T	Error C_T (%)
Fine	1.090	0.0732	-0.5
Coarse	1.0780	0.0724	0.6
Standard	1.0446	0.0701	3.7
Experiment	1.085	0.0729	-

3. Results and discussion

3.1. Aerodynamic analysis

The aerodynamic analysis was conducted for three different rotational speeds, including 4002 rpm, 5008 rpm and 6018 rpm, across a range of advance ratios. Experimental data showing the relationship between thrust coefficient and advance ratios at various rotational speeds are presented in **Table 4**.

Table 4. Experimental data of thrust coefficient versus advance ratios at various rotational speeds.

4002 rpm		5008 rpm		6018 rpm	
J	C_T	J	C_T	J	C_T
0.160	0.0792	0.129	0.0888	0.108	0.0939
0.195	0.0729	0.161	0.084	0.133	0.0915
0.234	0.0656	0.193	0.0787	0.160	0.0884
0.278	0.0578	0.224	0.0732	0.189	0.0840
0.315	0.0524	0.260	0.0662	0.213	0.0803
0.369	0.0445	0.290	0.0605	0.240	0.0754
0.397	0.0405	0.320	0.0545	0.270	0.0692
0.443	0.0337	0.354	0.049	0.296	0.0638
0.487	0.0262	0.388	0.0434	0.321	0.0588
0.527	0.0196	0.412	0.0396	0.347	0.0533
0.564	0.0128	0.448	0.0338	0.375	0.0480
0.602	0.0057	0.481	0.0283	0.400	0.0437
0.654	-0.0038	0.507	0.024	0.424	0.0397
-	-	0.547	0.0172	0.454	0.0346

The thrust coefficient results against various advance ratios from the CFD analysis were plotted at three different rotational speeds (4002 rpm, 5008 rpm and 6018 rpm) as shown in Figure 6–8. At 4002 rpm, the computational results showed differences from experimental data ranging between 0.3% and 96.7%, with larger discrepancies occurring at higher advance ratios. The analysis at 5008 rpm demonstrated better agreement, with differences between 0.2% and 23.1%. The best correlation was found at 6018 rpm, where the differences between CFD and experimental results ranged from 0.1% to 12.1%. Specifically, the results for the thrust coefficient showed a slight under-prediction for a low advance ratio at 4002 rpm, while the results showed over-prediction for higher advance ratios. At 5008 rpm, the CFD results showed a slight under-prediction at low advance ratios and the accuracy improved as the advance ratio increased. At 6018 rpm, the predictions remained below the experimental results at low advance ratios whereas the CFD results converged with the experiments at higher advance ratios. While there are some discrepancies between the experimental data and CFD results for the thrust coefficients at 4002 rpm, 5008 rpm and 6018 rpm, overall, the agreement is satisfactory. The observed discrepancies, particularly at higher advance ratios, can be attributed to several factors including the increased complexity of three-dimensional flow phenomena such as tip vortex interactions and blade-wake interactions that become more pronounced at higher advance ratios. The results observed at higher RPMs (6018 rpm) suggests that Reynolds number effects and flow predictability improve with increased rotational speed, while lower RPMs may be more susceptible to laminar-turbulent transition uncertainties and modeling limitations.

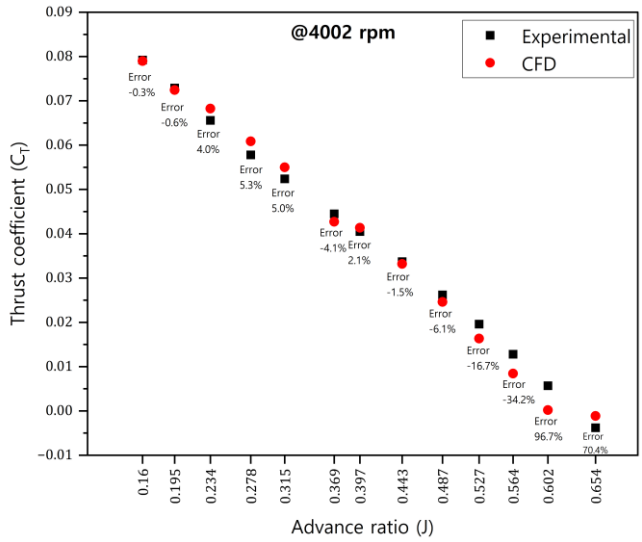

Figure 6. Thrust coefficient versus advance ratios at 4002 rpm.

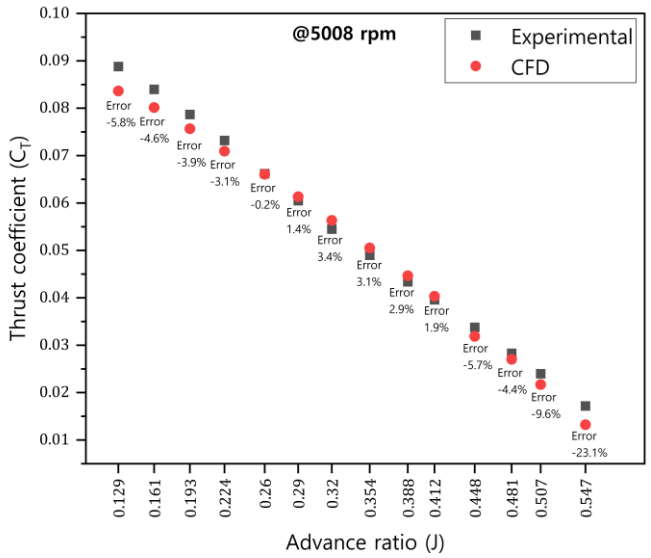

Figure 7. Thrust coefficient versus advance ratios at 5008 rpm.

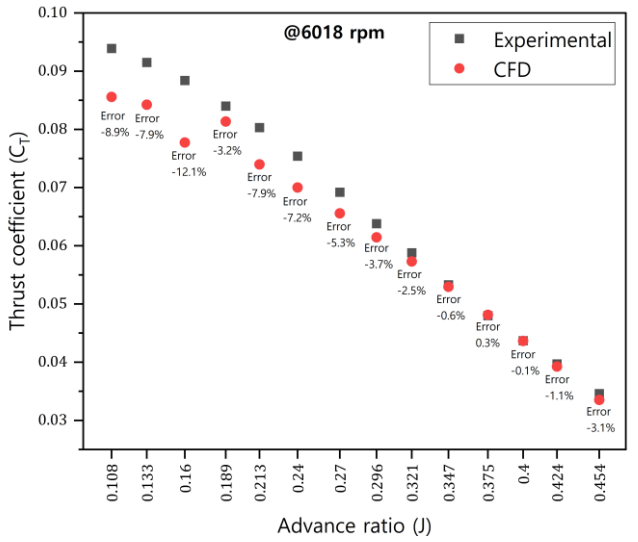

Figure 8. Thrust coefficient versus advance ratios at 6018 rpm.

3.2. Aeroacoustic analysis

The airflow was modeled as an ideal gas since it is a compressible fluid. The energy equation was also activated because the ideal gas properties depend on the temperature. The aeroacoustic analysis was performed at an advance ratio of 0.195 J and a rotational speed of 4002 rpm. For turbulence modeling, the LES method with the Wall-Adapting Local Eddy-viscosity (WALE) subgrid-scale model was chosen for acoustic calculations. LES directly resolves the large, energy-containing turbulent structures while using subgrid models to represent the smaller turbulent scales that cannot be captured by the computational mesh. The WALE model specifically improves accuracy near walls by adjusting the eddy-viscosity calculations to account for how turbulence behaves differently close to solid surfaces, where it becomes damped and changes structure (Hairudin et al., 2024). This LES approach offers a practical balance between computational cost and accuracy by solving the large turbulent eddies directly while modeling only the smaller dissipative scales, making it an efficient solution for turbulence simulations (Du Plessis and Bouferrouk, 2024). The QUICK numerical scheme was implemented for the solution methods, while the Flowcs Williams and Hawkings (FW-H) model served as the acoustics model to predict noise generation. A coarse mesh configuration was applied for the aeroacoustic analysis using the same element size. **Figure 9** illustrates the spatial distribution of receiver points positioned around the propeller for acoustic measurements.

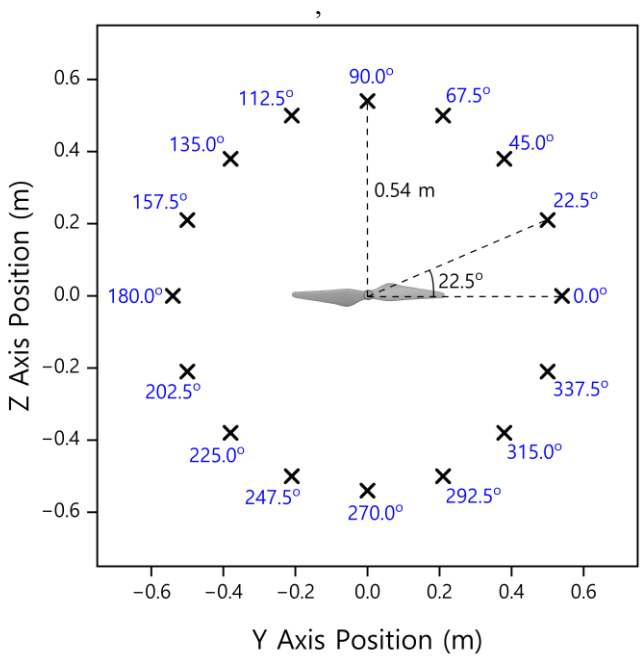

Figure 9. Receiver point locations.

The initial evaluation of the computational acoustic results focused on examining the overall sound pressure levels measured at multiple receiver positions surrounding the propeller. These measurements consolidate the acoustic intensity across all captured frequencies into single representative values enabling comprehensive analysis of sound propagation patterns throughout a complete 360° circumference around the propeller. **Figure 10** displays the distribution of overall sound pressure levels throughout the measurement domain. The acoustic analysis revealed sound pressure levels varying between 60.17 dB and 62.29 dB with the peak intensity occurring at the 22.5° position and minimum levels recorded at 225°. The relatively narrow range of measured sound pressure levels indicates moderate and well-controlled noise generation across all angular positions around the propeller, demonstrating favorable aeroacoustic characteristics for the propeller design.

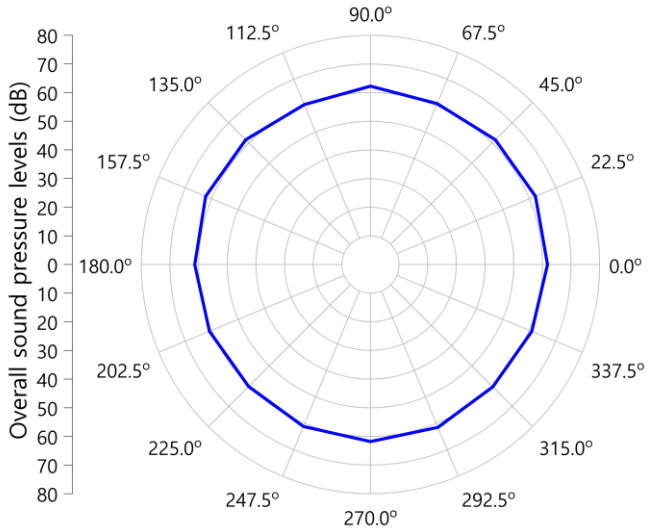

Figure 10. Overall sound pressure levels.

The detailed acoustic evaluation continued by examining sound pressure measurements from receiver locations positioned at 45° and 90° angles relative to the propeller. **Figure 11** presents the frequency spectrum analysis of raw sound pressure levels at these specific angular positions. The comparative analysis revealed minimal variation in noise characteristics between the two measurement locations with closely matching frequency responses. A notable peak in sound intensity was observed in the frequency band between 7150 Hz and 7220 Hz particularly at the 90-degree measurement position where the maximum sound pressure levels were recorded.

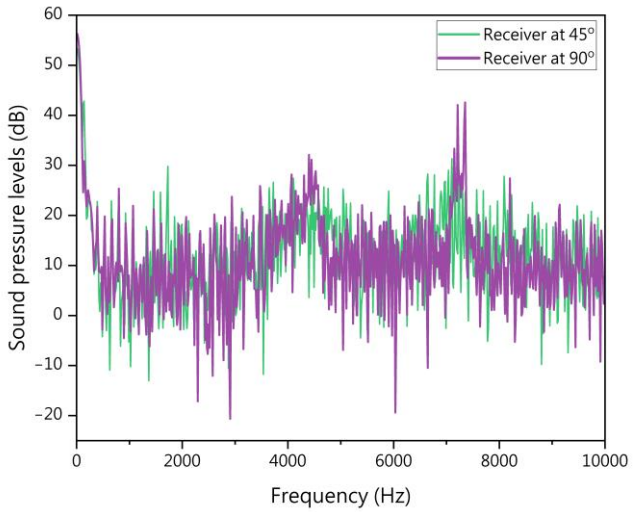

Figure 11. Raw sound pressure levels versus frequency for various positions.

The A-weighted sound pressure level analysis provides insight into the human perception of propeller noise by applying frequency-dependent corrections that match the sensitivity of human hearing. Figure 12 presents the A-weighted sound pressure levels across the frequency spectrum for measurements taken at the 45° and 90° positions. The A-weighting significantly reduces the contribution of low-frequency components while emphasizing the mid-frequency range where human hearing is most sensitive. This analysis reveals that the most significant noise components perceived by human observers occur in the frequency range between 7000-7500 Hz, with the 90° position, showing slightly higher a-weighted levels compared to the 45° position. The concentration of noise in the 7000-7500 Hz frequency range is significant for UAV urban operations as this range falls within the most sensitive portion of human hearing, making the propeller noise particularly noticeable and potentially annoying to urban residents. The frequency range of 315-1000 Hz shows relatively low noise levels (32-38 dB), suggesting that operational strategies could target these frequencies through rotational speed control to reduce overall noise signatures. The significant noise peaks in the higher frequency ranges (4000-8000 Hz) align with human hearing sensitivity and urban noise regulations, requiring targeted acoustic treatments or blade geometry modifications to mitigate these critical frequencies. The A-weighted analysis confirms the overall moderate noise characteristics of the propeller design, particularly in frequency ranges most relevant to human perception.

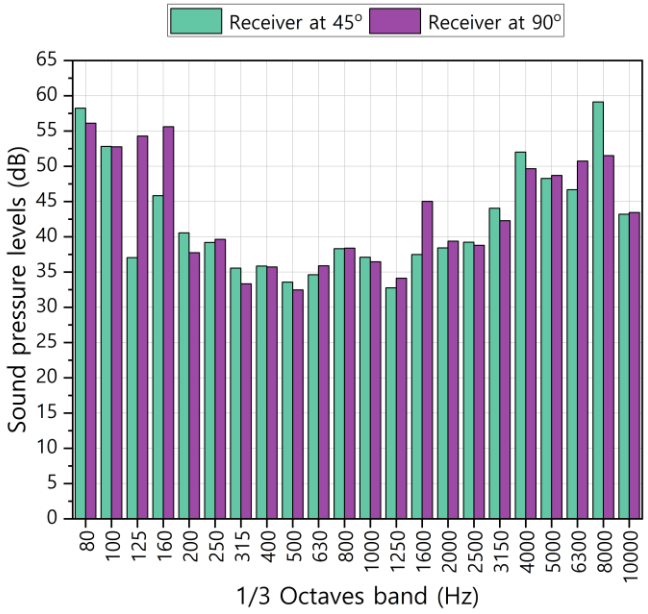

Figure 12. A weighted sound pressure levels versus frequency at various positions.

4. Conclusions

This research provides valuable insights into the aerodynamic and aeroacoustic characteristics of UAV propeller blades, offering compelling evidence for their potential in noise reduction applications. The study demonstrates that commercial CFD software serves as a reliable and cost-effective alternative to traditional experimental testing for initial performance predictions.

The investigation revealed distinct performance patterns across different operational conditions. The thrust coefficient analysis at various rotational speeds showed notable trends:

- At 4002 rpm, the CFD simulations slightly underestimated thrust values at low advance ratios while showing overestimation at higher advance ratios, with prediction errors ranging from 0.3% to 96.7%. This wide variance suggests that lower RPM operations may require conservative thrust predictions for flight safety margins.
- At 5008 rpm, it demonstrated improved predictive accuracy with errors between 0.2% and 23.1%,

showing particular improvement as advance ratios increased. This operational range provides more reliable performance predictions for mission planning applications.

- At 6018 rpm, it exhibited the strongest correlation between CFD predictions and experimental data, with error ranging from only 0.1% to 12.1%. This superior accuracy makes the higher speed range optimal for high-performance applications where precise thrust prediction is essential.

Despite minor variations between computational predictions and experimental measurements across all rotational speeds, the overall correlation proved satisfactory. The computational model successfully demonstrated its capability to predict small-scale propeller performance characteristics under low Reynolds number conditions.

The aeroacoustic analysis yielded particularly promising results, with propeller-generated noise levels remaining within a narrow band of 60.17 dB to 62.29 dB. The spatial distribution of noise showed systematic variation, with peak intensity recorded at the 22.5° position and minimum levels at the 225° position. These moderate noise levels across all angular positions indicate excellent acoustic performance, suggesting potential applications where noise reduction is a priority. In conclusion, these findings contribute valuable insights to the field of UAV propeller design and highlight the effectiveness of computational methods in predicting both aerodynamic and acoustic performance characteristics.

Based on the aeroacoustic findings, manufacturers should focus on blade tip design modifications to reduce the dominant noise frequencies in the 7000-7500 Hz range. The moderate noise levels (60.17-62.29 dB) indicate that current composite materials are adequate, but manufacturers should consider implementing damping materials or sandwich constructions to further attenuate structural vibrations that contribute to noise generation. Carbon fiber reinforced polymers with integrated damping layers could reduce both weight and noise while maintaining structural integrity. Manufacturers should implement strict tolerances for blade geometry, surface finish, and balancing to ensure consistent aeroacoustic characteristics across production units.

Conflicts of Interest

The authors declare that there is no conflict of interest regarding the publication of this paper.

References

Ahmad, F., Kumar, P., Dobriyal, R. and Patil, P. P. (2021). Estimation of the thrust coefficient of a Quadcopter Propeller using Computational Fluid Dynamics. IOP Conference Series: Materials Science and Engineering, 1116, 012095. p.

Ahmad, F., Kumar, P., Pravin, P. and Kumar, V. (2021). Design and modal analysis of a Quadcopter propeller through finite element analysis. International Conference on Technological Advancements in Materials Science and Manufacturing, 46, 10322–10328. pp.

Al-Haddad, L. A., Giernacki, W., Basem, A., Khan, Z. H., Jaber, A. A. and Al-Haddad, S. A. (2024). UAV propeller fault diagnosis using deep learning of non-traditional χ2-selected Taguchi method-tested Lempel–Ziv complexity and Teager–Kaiser energy features. Scientific Reports, 14(1), 18599. p.

Anh Vu, C. T., Van Hung, Phan, Dinh Chien ,Dang, Thai ,Vu Dang and and Quang, P. K. (2025). Improving energy efficiency for fishing vessels using two-pitch propellers. Journal of International Maritime Safety, Environmental Affairs, and Shipping, 9(1), 2460136. p.

Brandt, J. B. (2005). Small-scale propeller performance at low speeds. University of Illinois at Urbana-Champaign.

Çelebi, Y. and Aydın, H. (2025a). Multirotor Unmanned Aerial Vehicle Systems: An In-Depth Analysis of Hardware, Software, And Communication Systems. Journal of Aviation, 9(1), 225–240. pp.

Çelebi, Y. and Aydın, H. (2025b). Analysis of Directional Stability of A Quadcopter for Different Propeller Designs Using Experimental and Computational Fluid Dynamics Applications. Politeknik Dergisi, 1–1. pp.

Çelebi, Y., Cengiz, M. and Aydın, H. (2024). Propeller Design of UAV Under Low Reynolds Numbers. In Article and Reviews in Engineering Sciences (407–438. pp.). Platanus Publishing.

Céspedes, J. F. and Lopez, O. D. (2019). Simulation and validation of the aerodynamic performance of a quadcopter in hover condition using overset mesh. In AIAA Aviation 2019 Forum (Vol. 1–0). American Institute of Aeronautics and Astronautics.

Ciattaglia, G., Iadarola, G., Senigagliesi, L., Spinsante, S. and Gambi, E. (2023). UAV Propeller Rotational Speed Measurement through FMCW Radars. Remote Sensing, 15(1).

Cruzatty, C., Sarmiento, E., Valencia, E. and Cando, E. (2022). Design methodology of a UAV propeller implemented in monitoring activities. Advances in Mechanical Engineering Trends, 49, 115–121. pp.

de Carvalho, P. H., Cuenca, R. G. and da Silva, F. D. (2023). Cob-2023-1717 on the prediction of propeller tonal noise with machine learning. 27th ABCM International Congress of Mechanical Engineering.

Del Duchetto, F., Pagliaroli, T., Candeloro, P., Rossignol, K.-S. and Yin, J. (2025). Aeroacoustic Study of Synchronized Rotors. Aerospace, 12(2).

Du Plessis, J. and Bouferrouk, A. (2024). Aerodynamic and Aeroacoustic Analysis of Looped Propeller Blades. 3156. p.

Durmuş, S. (2024). Statistical Analysis of Airfoil Usage in Aircraft. Journal of Aviation, 8(3), 214–220. pp.

Eraslan, Y. and Oktay, T. (2021). Numerical Investigation of Effects of Airspeed and Rotational Speed on Quadrotor UAV Propeller Thrust Coefficient. Journal of Aviation, 5(1), 9–15. pp.

Hairudin, W. M., Mat, M. N. H., Ooi, L. E. and Ismail, N. A. (2024). Co-simulation approach for computational aero-acoustic modeling: Investigating wind-induced noise within two-way radio microphone ports cavity. Journal of Mechanical Engineering and Sciences, 18(1), 9909–9927. pp.

J. Lu, W. Nie, P. Xing, Z. Wang, Y. Cao, J. Wang, and Z. Xi. (2025). An EKF Based on Aerodynamic Constraints for Fixed-Wing AAV Attitude Estimation. IEEE Sensors Journal, 25(9), 14860–14874. pp.

Jin, J., Ye, Y., Li, X., Li, L., Shan, M. and Sun, J. (2025). A Deep Learning-Based Mapping Model for Three-Dimensional Propeller RANS and LES Flow Fields. Applied Sciences, 15(1).

Jordan, W. A., Narsipur, S. and Deters, R. (2020). Aerodynamic and Aeroacoustic Performance of Small UAV Propellers in Static Conditions. In AIAA AVIATION 2020 FORUM (Vol. 1–0). American Institute of Aeronautics and Astronautics.

Lasota, M., Šidlof, P., Kaltenbacher, M. and Schoder, S. (2021). Impact of the Sub-Grid Scale Turbulence Model in Aeroacoustic Simulation of Human Voice. Applied Sciences, 11(4).

Li, J., Zhang, M., Tay, C. M. J., Liu, N., Cui, Y., Chew, S. C. and Khoo, B. C. (2022). Low-Reynolds-number airfoil design optimization using deep-learning-based tailored airfoil modes. Aerospace Science and Technology, 121, 107309. p.

McKay, R. S., Kingan, M. J., Go, S. T. and Jung, R. (2021). Experimental and analytical investigation of contra-rotating multi-rotor UAV propeller noise. Applied Acoustics, 177, 107850. p.

Nikolaou, E., Karatzas, E., Kilimtzidis, S. and Kostopoulos, V. (2025). Winglet Design for Class I Mini UAV—Aerodynamic and Performance Optimization. Engineering Proceedings, 90(1).

Oktay, T. and Eraslan, Y. (2020). Computational fluid dynamics (Cfd) investigation of a quadrotor UAV propeller. 1–5. pp.

Özen, E. and Oktay, T. (2024). Maximization of Flight Performance of Eight-Rotor Multirotor with Differentiated Hub Angle. Journal of Aviation, 8(3), 206–213. pp.

Yıldırım Dalkıran, F. and Kırteke, E. (2024). Design and Implementation of A Low-Cost Parachute Landing System for Fixed-Wing Mini Unmanned Aerial Vehicles. Journal of Aviation, 8(3), 198–205. pp.

You, K., Zhao, X., Zhao, S.-Z. and Faisal, M. (2020). Design and Optimization of a High-altitude Long Endurance UAV Propeller. IOP Conference Series: Materials Science and Engineering, 926(1), 012018. p.

Cite this article: Celebi, Y., Aydin, A., Aydin, S. (2025). Computational Evaluation of Aerodynamics and Aeroacoustics of a Propeller for a Multirotor Unmanned Aerial Vehicle. Journal of Aviation, 9(2), 277-284